Noise prediction for increasingly complex jets. Part II: Applications

by

Michael L. Shur, Philippe R. Spalart and Michael Kh. Strelets

reprinted from

international journal of

aeroacoustics

volume 4 · number 3+4 · 2005

published by MULTI-SCIENCE PUBLISHING CO. LTD.,

5 Wates Way, Brentwood, Essex, CM15 9TB UK

E-MAIL: mscience@globalnet.co.uk

WEBSITE: www.multi-science.co.uk

international journal of aeroacoustics volume 4 · number 3&4 · 2005 – pages 247 – 266

Noise prediction for increasingly complex jets. Part II: Applications

Michael L. Shur*, Philippe R. Spalart, and Michael Kh. Strelets*****

*"New Technologies and Services" (NTS), St.-Petersburg 197198, Russia; mshur@rscac.spb.ru

**Boeing Commercial Airplanes, P.O. Box 3707, Seattle, WA 98124, USA; philippe.r.spalart@boeing.com

***"New Technologies and Services" (NTS), St.-Petersburg 197198, Russia; strelets@mail.rcom.ru

ABSTRACT

The numerical system described in Part I (Ref. 1) is applied to a variety of cases which increase difficulty, and progress in the direction of the complete simulation of an airliner engine. The grids have on the order of 1 million points. In many cases, the system meets the 2-3 dB accuracy target both in terms of directivity and of spectrum, up to a Strouhal number of about 1.5. The jet Mach number is varied from 0.3 to slightly supersonic with under-expansion, generating shock cells and greatly increasing side-line noise. For heated jets, the cross-effect between the acoustic Mach number and the temperature is correctly reproduced. Jets placed in a co-flowing stream with velocity up to 60% of the jet's are studied and found to sustain natural transition without unsteady forcing; the noise trends are correct. Finally, "synthetic chevrons" are added by altering the inflow conditions, and found to reduce low-frequency noise while increasing mid-frequency noise. In total, about fifteen meaningfully different cases are presented, and subjected to quantitative comparisons over the direction/frequency space without major failure. The principal limitation of the large-eddy-simulation approach remains its upper limit on frequency.

1. INTRODUCTION

In this paper, the methodology for jet noise prediction presented in detail in the first part (Ref. 1) is exercised on a variety of jets covering a wide range of physical factors. These include: effect of the Mach number for isothermal jets, effect of jet heating at low and high subsonic velocities, effect of forward flight at co-flow velocities up to the cruise range of airliners, effect of shock cells generated by under-expanded sonic jets, and, finally, effect of a chevron nozzle. A major goal of the study is to evaluate the capabilities of the approach in terms of adequate representation of all these effects. This is essential for an assessment of the readiness of the methodology for prediction of the noise of jets from real aircraft engines, which typically include a combination of all the listed factors and some additional ones (dual jets, nacelle, core plug, swirl, vane wakes, high core turbulence, etc.).

In Section 2 below we introduce the cases considered and present specific data on the grids and numerical parameters used in the LES of turbulence and the acoustic post-processing. In Section 3 we discuss the results of the simulations and compare them with experimental data (some of the results are available also in an earlier brief publication (Ref. 2), but with a much lower level of detail and interpretation). Finally, in the conclusion, we summarize the findings of the study, and outline future work.

2. DETAILS OF NUMERICS AND ACOUSTIC POST-PROCESSING

The matrix of cases is presented in *Table 1*. Notations used there are as follows. U_j and T_j are the values of the velocity and temperature at the nozzle exit (fully expanded values in the case of the sonic under-expanded jet, Case 16); p_j is the pressure at the nozzle exit; c is the speed of sound; M_a is the acoustic Mach number (fully expanded value in Case 16), and M is the actual Mach number at the nozzle exit; U_{CF} is the flight (co-flow) velocity; $\mathrm{Re} = \rho_j U_j D/\mu_j$ is the Reynolds number based on the jet diameter and exit flow parameters; σ_{min}^{upw} is the value of the weight of the upwind scheme in the turbulent jet region (see Section 3.1.1 in Ref. 1). Subscript "0" refers to the ambient air. Finally, the columns "Limiters" and "Expt." refer to the use of the flux limiters (see below) and to reference(s) to experimental studies (if available).

The grids used in all the cases have the same two-block topology described in detail in Ref. 1. However, in different cases they differ from each other in terms of domain size and grid-step distribution.

The static jets (Cases 1-7) are computed with the use of the grid shown in Ref. 1 (see Fig. 1 there). It is non-uniform in all three directions (except for the azimuthal direction in the outer block). The streamwise step at the nozzle exit, $\Delta x_{\min}$, is equal to $0.03D$, and the stretching factor in the turbulent region of the jet downstream of the potential core ($10 < x/D < 31$) is 1.013 (the minimum and maximum steps in this region are $0.11D$ and $0.3D$, respectively). In the lateral planes, the grid is nearly uniform in the inner Cartesian block, but is stretched in the radial direction in the outer cylindrical block. At the nozzle exit the near-wall $r-$step is equal to $0.003D$ (this small step is needed to resolve the incoming boundary layer) and its maximum value inside the nozzle is equal to $0.025D$. Outside the nozzle, the $r-$grid first stretches slowly in order to ensure a small step in the vicinity of the FWH control surfaces (Δr is less than $0.16D$ up to $r = 4D$) and then grows more rapidly, reaching the value of $2D$ at the outer boundary of the domain. Downstream of the nozzle, the radial grid gradually becomes more uniform due to the removal of the "wake" of the fine grid strip in the vicinity of the nozzle wall. As a result, the maximum radial grid step at the FWH surface (see Fig. 4 in Ref. 1) is nowhere larger than $0.15D$, and is smaller than $0.08D$ in the initial jet region, where most of the high-frequency noise is generated. Counting a minimum of about six cells to resolve a wavelength, with differencing schemes or 4^{th}- and 5^{th}-order accuracy, this sets a limit on the Strouhal number: $St < 2/M_a$, approximately.

For the jets with co-flow (Cases 9-13 in *Table 1*), the computational grids (and FWH surfaces) are narrowed down and elongated, to match the slower growth rate of such jets (the eventual scaling of the turbulent jet width is proportional to $x^{1/3}$, instead of x).

Table 1 **Matrix of Cases**

No.	$M_a = \frac{U_j}{c_0}$	M	$\frac{T_j}{T_0}$	$\frac{p_j}{p_0}$	$\frac{U_{CF}}{U_j}$	Re	**Grid (cells in outer and inner blocks)**	$\sigma_{\min}^{upw}$	**Limiters**	**Expt.**
Static subsonic isothermal jets										
1	0.9	0.9	1.0	1.0	0.0	10^4	(240×69×64)+ (216×16×16)	0.25	No	[3], [4]
2	0.57	0.57	1.0	1.0	0.0	10^4	(240×69×64)+ (216×16×16)	0.25	No	[3]
3	0.5	0.5	1.0	1.0	0.0	10^4	(240×69×64)+ (216×16×16)	0.25	No	[4]
4	0.36	0.36	1.0	1.0	0.0	10^4	(240×69×64)+ (216×16×16)	0.25	No	[3]
5	0.9	0.9	1.0	1.0	0.0	5×10^5	(240×69×64)+ (216×16×16)	0.25	No	[3], [4]
Static subsonic heated jets										
6	0.9	0.49	3.4	1.0	0.0	10^4	(240×69×64)+ (216×16×16)	0.25	No	[4]
7	0.5	0.27	3.4	1.0	0.0	10^4	(240×69×64)+ (216×16×16)	0.25	No	[4]
8	1.25	0.77	2.66	1.0	0.0	5×10^5	(317×66×64)+ (297×16×16)	0.25	No	[6]
Jets in co-flow, simulating forward flight										
9	0.9	0.9	1.0	1.0	0.1	5×10^5	(281×58×64)+ (261×16×16)	0.3	No	[5]
10	0.9	0.9	1.0	1.0	0.2	5×10^5	(281×58×64)+ (261×16×16)	0.35	No	[5]
11	0.9	0.9	1.0	1.0	0.3	5×10^5	(281×58×64)+ (261×16×16)	0.4	No	No
12	0.9	0.9	1.0	1.0	0.6	5×10^5	(370×55×48)+ (350×12×12)	0.5	No	No
13	1.25	0.77	2.66	1.0	0.21	5×10^5	(317×66×64)+ (297×16×16)	0.4	No	[6]
Jet with "synthetic chevrons"										
14	0.9	0.9	1.0	1.0	0.0	10^4	(240×69×64)+ (216×16×16)	0.25	No	No
Supersonic perfectly expanded and sonic under-expanded jets										
15	1.37	1.37	1.0	1.0	0.0	5×10^5	(317×66×64)+ (297×16×16)	0.25	Yes	[4], [7]
16	1.37	1.0	1.0	1.61	0.0	5×10^5	(386×83×48)+ (364×12×12)	0.25	Yes	[7]

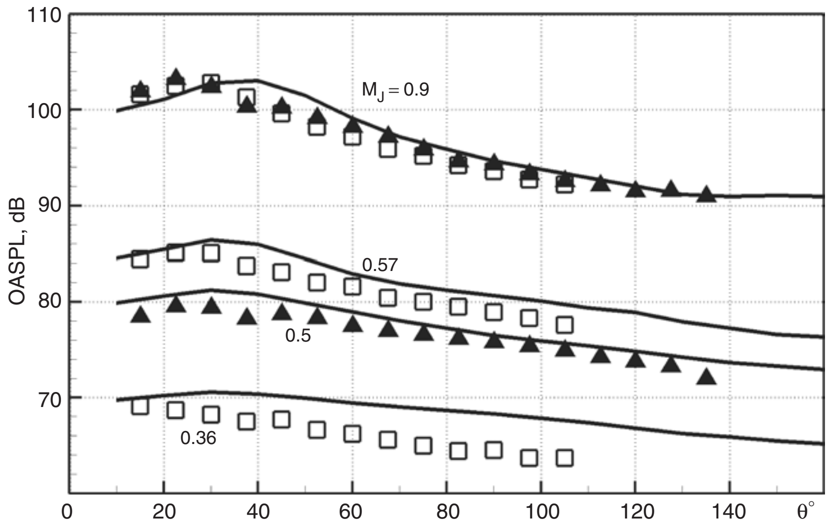

Figure 1. Directivity of noise over a range of Mach numbers for isothermal jets. Experiments from Lush [3] (squares) and Tanna [4] (triangles). Distance 120 diameters.

Also, the grid stretching in the streamwise direction is slower than in the static jets in order to keep a small $x-$step over a longer region in accordance with the increased length of the potential core. For instance, with the most intense co-flow (Case 12) the length of the domain is equal to $80D$, and Δx stays less than $0.2D$ up to $x/D = 45$.

The grid for Case 14 (emulated chevron nozzle) is a minor modification of the grid used for the other subsonic static jets (a description is presented in Subsection 3.4). Finally, for the under-expanded sonic jet (Case 16), the grid was perceptibly refined in order to enhance the resolution of shocks in the initial jet region. In particular, the $x-$step is equal $0.01D$ at the nozzle exit, and is kept less than $0.06D$ up to $x = 8D$.

As far as numerics are concerned, essentially, they are unchanged in all the simulations and correspond to those presented in detail in Ref. 1. The minor changes reflected in *Table 1* are associated with peculiarities of the specific problems considered. Namely, for the jets with co-flow, we use somewhat stronger upwinding (larger $\sigma_{\min}^{upw}$) which was found to be necessary to avoid oscillations in the acoustic pressure in the near–field of the turbulent region of the jet. Other than that, in order to avoid numerical instability in the simulations of the sonic and supersonic jets (Cases 15, 16), we use flux limiters in the upwind part of the approximations of the inviscid fluxes in the region of strong shock unsteadiness ($4<x/D<8$, $0.1<r/D<0.1+0.025\,(x/D-4)$ and $0.5<x/D<8$, $0.1<r/D<0.1+0.02\,(x/D-0.5)$ for Cases 15 and 16, respectively).

The time steps in the simulations vary in the range from $0.02D/U_j$ to $0.03D/U_j$ (this corresponds to a Courant number based on the jet velocity and minimal $x-$step less than 2), and the number of sub-iterations within each time step in different cases varies from 8 to 12, which is sufficient for a nearly 3-orders-of-magnitude drop of the residuals. As for the time samples needed to obtain statistically mature turbulent and acoustics fields, they depend on the run initialization. For instance, if the simulation is started from scratch, based on our experience, a sufficient time sample is about 800 convective time units, D/U_j. However, if a realistic initial field is available (e.g., from a mature solution for the same jet obtained on a coarser grid), the time sample may be significantly reduced (roughly by half). As a result, the number of time steps in the simulations varies from 15,000 up to 30,000, which, depending on the grid, takes from 3 weeks to 2 months of CPU time on a dual-processor PC, rated at 2.8gHz.

Once a mature turbulent field is obtained, the code starts collecting the data needed for the acoustic post-processing (see Ref. 1 for details), which demands running 200-300 additional convective time units (the data are stored with a time step of around 0.2 convective units, thus setting an absolute limit of 2.5 for the Strouhal number). Note that these relatively short acoustic samples are sufficient only provided that the sound pressure level is averaged over enough azimuthal directions (typically over 32 azimuthal angles, φ, in our post-processing).

The acoustic data are stored on 9-15 nested FWH surfaces. This is needed for averaging of the closing disks (see Section 3.2.6 of Ref. 1) and, also, is very helpful for an a posteriori analysis of the noise surface-sensitivity. Note that the typical CPU time needed for the acoustic post-processing is rather short (not more than 6 hours), which makes it possible to analyze the noise prediction routinely in the course of simulations, and to adjust the control surfaces in case they are sub-optimal.

3. RESULTS AND DISCUSSION

In this section, we present major results of the simulations of the jets listed in *Table 1*. The discussion is organized as follows. In Subsection 3.1 we consider the effect of the Mach number on the isothermal static jets (Cases 1-4 in *Table 1*). Then, we explore Cases 1, 3, 6, 7 in order to evaluate the effect of jet heating at high (Cases 1, 6) and low (Cases 3, 7) jet velocity. Subsection 3.3 is devoted to an assessment of the methodology as applied to isothermal and hot jets in forward flight (Cases 5, 9-12 and 8, 13). In Subsection 3.4 we describe a procedure developed for the emulation of chevron nozzles via an appropriate modification of the velocity field at the nozzle exit, and present a comparison of the simulations of Cases 1 and 14, to assess the efficiency of chevrons for noise reduction. Finally, in Subsection 3.5 we present perfectly-expanded supersonic and under-expanded sonic jets (Cases 15, 16), to evaluate the impact of broadband shock-cell noise.

For most of the cases, restricted grid-sensitivity studies were carried out, with grids having roughly half the number of cells of those described in Section 2 above. The studies showed that in this range, the sensitivity is quite moderate, although for strongly heated jets and jets with high co-flow velocity, the difference in the noise prediction betwen the “fine” and “coarse” grids can reach 2-3 dB.

3.1. Effect of Mach-number on isothermal subsonic jets

An examination of the jet flow-patterns at different Mach numbers (not shown) does not reveal significant differences in terms of either turbulence and sound-wave structure

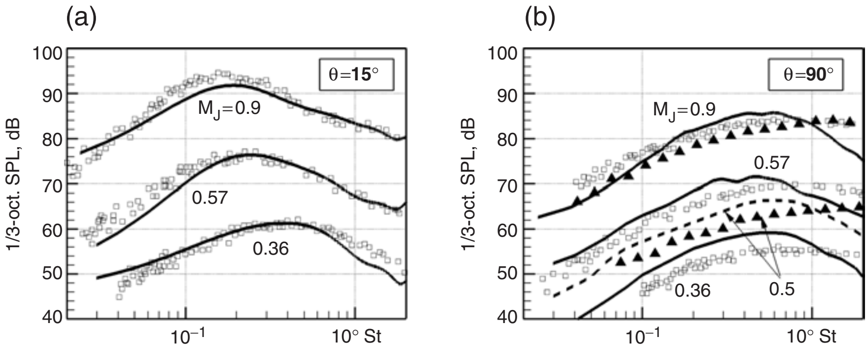

Figure 2. Effect of Mach number on 1/3-octave spectra at two observer angles. Notations as in Fig. 1.

or mean flow characteristics (e.g., length of the jet potential core and its width). The simulations also roughly confirm Lighthill's scaling law for the acoustic pressure, $p' \sim U_j^4$.

The effect of Mach number on jet noise is seen in Figs. 1, 2 where we present computed overall sound pressure level (OASPL) directivity curves and 1/3-octave intensity spectra at four Mach numbers, together with the experimental data of Lush [3] and Tanna [4]. In general, the comparison with the data on the OASPL is satisfactory, although at $\theta = 90°$ this is partially dependent on the cancellation of errors between an excess at low frequencies and a deficit at frequencies higher than $St \approx 1$ (see Fig. 2 and the discussion of this issue in Section 4 of Ref. 1).

As expected from theory, lower Mach numbers give noise levels that are much lower, and more uniform over the directions. Lower speeds also make the numerical problem more difficult, by widening the intensity gap between the sound waves and the turbulence (the gap is wider by a factor of over 30 at Mach 0.36 than at Mach 0.9). It is plausible that this is the reason the disagreement at the lowest Mach, 0.36, exceeds 4 dB in OASPL and 5 dB in the spectra at 90° observer angle. Nonetheless, the computed spectra correctly reproduce the experimental behavior of the peak non-dimensional frequency over the entire Mach-number range considered (it drops as M^{-1} at small observer angles, and remains nearly constant at the direction normal to the jet axis). The figures also give a reminder of the difference in peak-level angle relative to two sets of experiments at Mach 0.9, mentioned in Section 4 of Ref. 1.

3.2. Cross-effect between jet acoustic Mach number and temperature

The prevailing view based on experiments (see, for example, Refs. 8, 9, 4) is that the effect of jet heating on noise is opposite for high- and low-velocity jets. Namely, for the same jet velocity, a higher temperature reduces noise if $M_a > 0.7$, but increases it if $M_a < 0.7$. Still, the latter fact remains a subject of considerable debate (see Refs. 10, 11), and we are not aware of other attempts to clarify this question with the help of

Table 2 **Effect of jet heating on the major mean and turbulent jet parameters, and comparison with experiments**

Jet Parameters		x_{CU}/D 1)		x_{CT}/D 2)	x_{CT}/x_{CU}		B_u 3)		$(u'_{CL})_{max}/U_j$	
T_j	M_a	Pred	Exp	Pred	Pred	Exp	Pred	Exp	Pred	Exp
1	0.5	4.7	4.5-5.0 [12],	-	-	-	6.8	5.4-6.1 [16],	0.13	0.13 [12]
	0.9	4.8	[14]	-	-	-	6.55	~7 [14]	0.13	0.12 [12]
3.4	0.5	3.2	3.1-3.5 [12],	2.7	0.85	0.77 [12],	4.1		0.17	-
	0.9	3.6	2.5-3.0 [14]	3.1	0.86	~0.73 [14]	4.05	~4.5 [14]	0.17	0.17 [12]

1)length of the dynamic jet core, defined as the distance from the nozzle exit to the point where the mean centerline velocity normalized with the jet velocity U_{CL}/U_j falls down to 0.98; 2)length of the thermal jet core, defined as distance from the nozzle exit to the point where the relative normalized temperature $\Theta_{CL} = (T_{CL} - T_0)/(T_j - T_0)$ falls down to 0.98;

3)rate-coefficient of the centerline velocity decay in the developed jet region: $U_{CL}/U_j = B_u D/(x - x_0)$.

LES-based numerical approaches to noise prediction. In the present study, we address this issue through a comparison of the noise predictions for two ($M_a = 0.9$ and $M_a = 0.5$) hot ($T_j/T_0 = 3.4$) jets with the corresponding predictions for isothermal jets ($T_j/T_0 = 1.0$) at the same values of M_a. However, before presenting noise results, it is instructive to compare turbulent characteristics of hot jets from our simulations with the experimental data of Lau [12], Lockwood and Moneib [13], and Simonich *et al* [14] (although the experiments were carried out at somewhat different values of M_a and T_j/T_0 from those in the simulations, it should not strongly affect the comparison of the normalized quantities we are performing).

As seen in *Table 2* and Figs. 3-5, the simulations do capture the major physical features of hot jets observed in experiments. In particular, for the mean flow, they reveal a significant diminution of the jet dynamic potential core at elevated temperatures, and suggest that the length of the dynamic core in the hot jets is larger than that of the thermal potential core (see Fig. 3 and *Table 2*). Also, just as in the experiment of Lau [12], in the simulations heating causes a turning of the shear layers towards the jet axis, which is seen in the mean streamwise velocity contours in Fig. 3c,d (the “inner” part of the shear layers is wider, while its “outer” part remains virtually unchanged). Also in line with experiments, the simulations predict a faster damping of turbulence in the hot jets (see Fig. 3a,b). Figures 4, 5a demonstrate fairly good agreement between simulations and data on the distribution of the non-dimensional mean streamwise velocity along the jet centerline, U_{CL}/U_j (the predictions are well within the

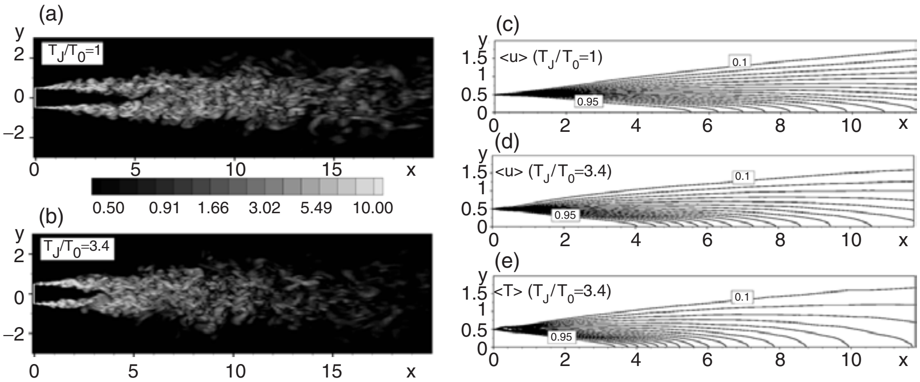

Figure 3. Effect of jet heating on instantaneous vorticity (a, b) and time-average axial velocity and relative temperature (c-e), with acoustic Mach number 0.5.

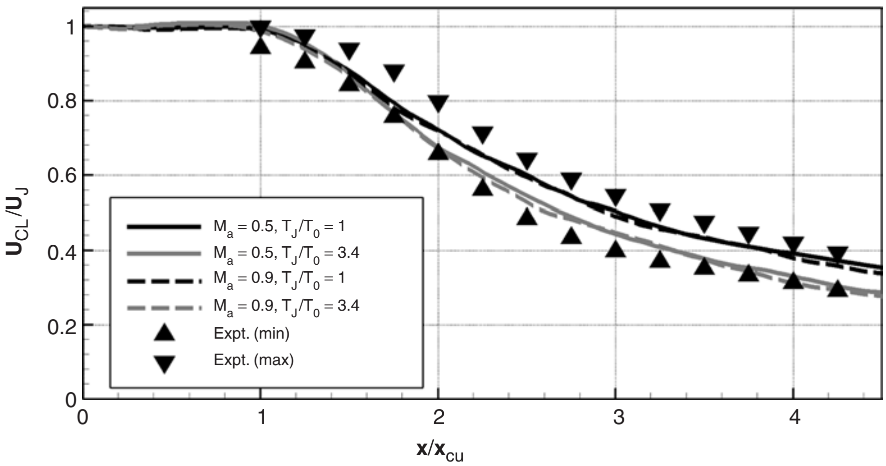

Figure 4. Effect of acoustic Mach number and jet temperature on normalized centerline distribution of mean axial velocity. Experiments from Lau [12].

experimental scatter) and on the radial profiles of the relative temperature Θ normalized with its centerline value, Θ_{CL}.

For turbulence statistics, simulations quite accurately predict the experimental value of the peak of velocity fluctuations on the jet axis and its increase with heating (*Table 2*). Also similar to experiments of Refs. 12, 15 the fluctuation distributions (not shown) peak at a distance of about two potential core lengths from the nozzle. Finally, the radial profiles of the normalized root-mean square of the temperature fluctuations (Fig. 5b) are within the scatter of the available experimental data.

We can conclude that, as far as the mean-flow characteristics and one-point turbulence statistics are concerned, the agreement between simulations and experiments

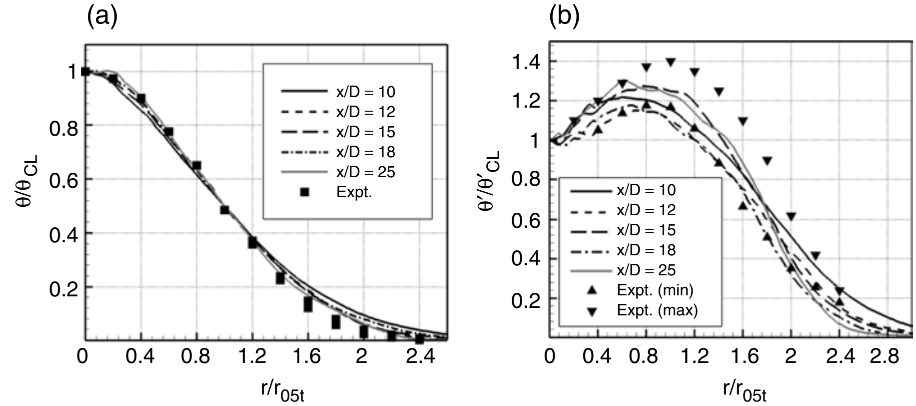

Figure 5. Normalized radial distributions of mean relative temperature (a) and temperature fluctuations (b) in developed jet region for $M_a = 0.9$ and $T_j/T_0 = 3.4$. Experiments from Lockwood and Moneib [13]; r_{05t} is the "temperature-based" jet half-radius, i.e., distance from the axis to the point where $\Theta/\Theta_{CL} = 0.5$

is quite satisfactory. However, since noise generation can be viewed as driven by two-point turbulence statistics, the present statistics are not sufficient to predict the effects on noise.

For the noise prediction, the simulations appear to capture the relatively subtle cross-effect of jet heating and acoustic Mach number rather well. In particular, they do support the experimental observations that jet heating results in a noticeable noise increase at low jet velocities, and a reduction at high velocities. This is seen in Fig. 6a, where the corresponding OASPL directivity plots are compared with each other and with the experimental data of Tanna [4]. More specifically, the plots show that at

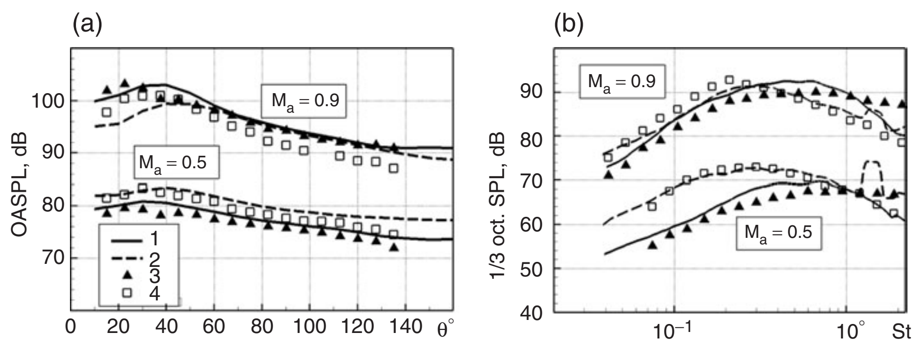

Figure 6. Noise directivity and 1/3-octave spectrum at $\theta = 45°$ with different jet temperatures and acoustic Mach numbers: 1, 2 – simulations, 3, 4 – experiments from Tanna [4]; 1, 3 – $T_j/T_0 = 1$; 2, 4 – $T_j/T_0 = 3.4$. Distance 120 diameters.

$M_a = 0.5$, according to both simulations and experiments, jet heating causes an increase of the sound intensity at all observer angles, while at $M_a = 0.9$ it results in a drop. However, in the simulations this drop is visually pronounced only for θ varying in the range 0°-60° while for 60°-130° the two directivity curves virtually coincide. In the experiment, a relatively strong drop of the sound intensity, although also rather non-uniform, is observed in a wider range of observer angles (it is negligible only for $40° < \theta < 60°$). Thus, at $M_a = 0.9$, the heating effect is almost missed for the sideline noise; this may originate in smaller scales of motion, which are not supported by the present grid.

For the 1/3-octave spectra, quite in line with experimental observations, the simulations predict a shift of the noise generated by hot jets to the low-frequency range (see Fig. 6b). The quantitative agreement between the computed and measured spectra is also fairly good: the discrepancy does not exceed 2 dB, except for the false "bumps" near $St \approx 1.5$. These originate from sharp spurious peaks in the raw spectra, which, in turn, are caused by the excessively axisymmetric character of the flow in the transitional region, as discussed in Ref. 1.

3.3. Co-flow, simulating jets in flight

The capability of correctly capturing this effect is obligatory for any numerical tool with claims over aircraft jet-noise prediction. However, as mentioned in Ref. 1, in the absence of unsteady inflow perturbations, there was a concern that the global instabilities, which sustain transition, would disappear once the fluid outside the jet was streaming fast enough relative to the nozzle (as in flight), thus defeating the simple approach free of arbitrary jet forcing. Fortunately, the concern turned out to be unjustified (although the simple fact that transition still occurs does not guarantee that it remains physically realistic). This is seen in Fig. 7, where we show instantaneous vorticity fields from the simulations of isothermal $M = 0.9$ jets with different co-flow levels (Cases 5, 9-12 in *Table 1*). The increase of the co-flow results in a visible stabilization of the shear-layer

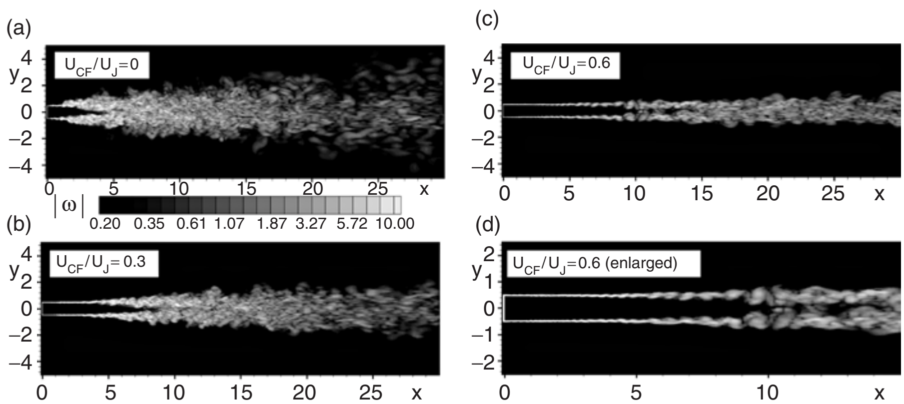

Figure 7. Vorticity of jets without and with co-flow.

and an extension of the length of the jet potential core up to $\approx 12D$ at $U_{CF} = 0.6U_j$. Nonetheless, transition to turbulence does occur even at this high value of the co-flow ratio. The roll-up of the shear layer is coarser, which could result from its viscous thickening, and the grain of the turbulence is not as fine as it is without co-flow. This finding could be related to two factors: upwind-biased differencing errors are somewhat stronger with co-flow; and the turbulence cascade is less powerful, which reduces the energy supply to small eddies. The persistence of transition is reassuring, since the value of the ratio reaches about 0.65 for the fan flow of an airliner (ground-based experiments have not gone past about 0.3 for realistic jet Mach numbers, Ref. 5). Note that the Reynolds number in this series was raised, which had no influence in the jet itself, but was needed to avoid forming too thick a boundary layer on the outside wall of the nozzle.

Figure 8a shows a comparison of the non-dimensional centerline turbulence intensity over a wide range of co-flow velocities with the experimental data of Morris [17]. The agreement with experiment is again reasonably good, although the peak values of the intensity are underestimated by up to 15-20%, and the centerline activity within 2 diameters of the nozzle is visibly lower (this is a consequence of the inflow condition). An interesting feature revealed by the simulation at $U_{CF} = 0.6U_j$ is the non-monotonic variation of the turbulence intensity, with a local maximum at $x/x_c \approx 0.8$. This seems consistent with the nearly axisymmetric character of the shear layer roll-up, and vortex pairing near the end of the jet potential core (see Fig. 7d). Unfortunately, experimental data are not available at such high values of U_{CF}, but the visual trend towards the formation of this maximum is quite pronounced in the experiment of

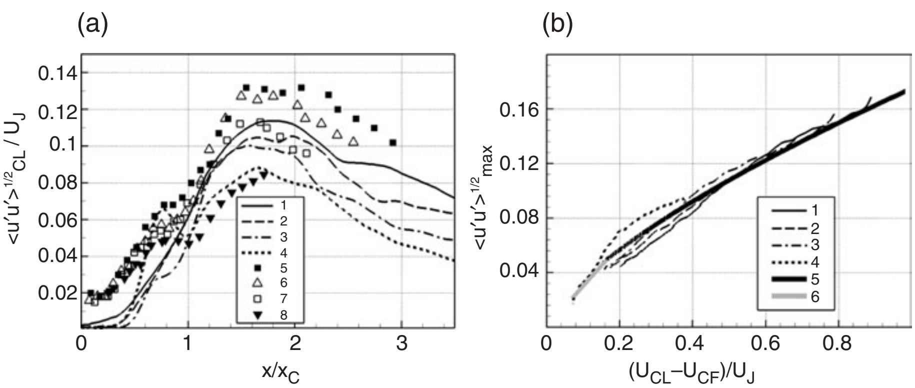

Figure 8. Normalized centerline axial turbulence intensity (a) and its peak value in the shear-layer (b) with different co-flow velocities. (a): 1 – 4 – CFD at $M = 0.9$, ratio 0.1, 0.2, 0.3, and 0.6; 5 – 8 – experiments of Ref. 17 at $M = 0.47$, ratio 0.096, 0.206, 0.305, and 0.497. (b): 1 – 4 – as in frame (a); 5, 6 – analytical fits of Ref. 17 at high and low values of parameter $b = (U_{CL} - U_{CF})/U_j$: $0.175b^{0.7}$ (for $b > 0.163$) and $0.3b$ (for $b < 0.163$), respectively.

Ref. 17 already at $U_{CF} = 0.497U_j$. Finally, as shown in Fig. 8b, the computed dependence of the maximum turbulence intensity on the parameter $(U_{CL} - U_{CF})/U_j$ for all the considered co-flow velocities agrees reasonably well with the two-branch analytical fit suggested by Morris [17] on the basis of his own experimental data and those of Ref. 18.

Before moving on to noise predictions with different co-flow levels, it should be noted that in the experimental studies performed in flight ("flyover experiments") and in laboratory environments (wind tunnel or "flight simulation experiments") the results of noise measurements are somewhat contradictory. Namely, at small angles to the jet exhaust (rear arc, emission angles $\theta_e < 90°$) both types of experiments show a noise reduction with increased co-flow intensity. However at $\theta_e > 90°$ (forward arc) they give quite different results: the flight-simulation experiments still show a significant noise reduction, while virtually all the flyover tests demonstrate either no change or an increase of the noise in comparison with the static conditions. An explanation of that inconsistency found in the literature (e.g., Refs. 19, 5, 6) is that in flight, additional noise sources ("internal" engine noise, turbulence of external boundary layer, etc.) may dominate the jet noise in the forward arc. Since our simulations do not contain those additional noise sources, the conditions we are reproducing in CFD are closer to the laboratory flight-simulation experiments. Therefore, we compare the predictions with such experiments (Refs. 5 and 6).

In particular, Fig. 9 compares predicted sound levels with the experiments of Ref. 5 (the data for the static jet are from Ref. 4). The agreement is satisfactory, although the

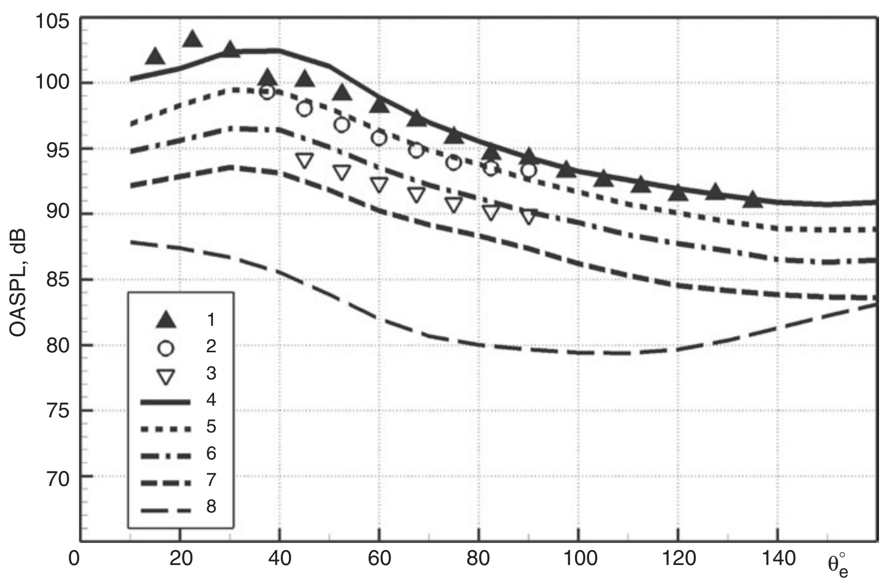

Figure 9. Sound directivity with different co-flow ratios at $M = 0.9$. 1 – experiments of Ref. 4, ratio 0; 2, 3 – experiments of Ref. 5, ratio 0.11 and 0.22; 4 – 8 – CFD, ratio 0, 0.1, 0.2, 0.3, 0.6. Distance 120 diameters.

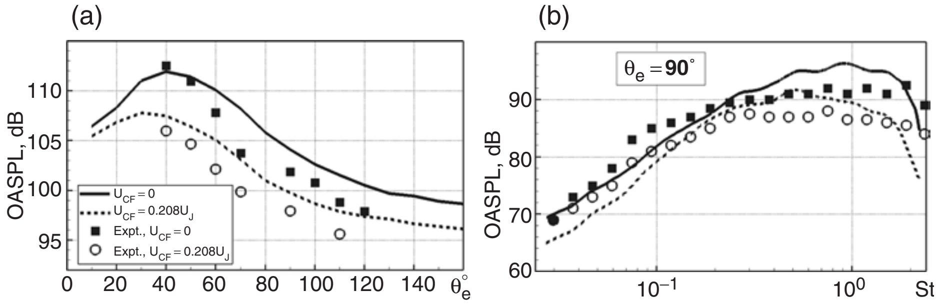

Figure 10. Effect of co-flow on noise directivity and 1/3-octave spectrum at $\theta_e = 90°$ for hot jet of Ref. 6. Distance 100 diameters.

data are available only in a restricted range of co-flow intensities ($U_{CF} \leq 0.22U_j$) and emission angles ($\theta_e = 40° \div 90°$). The effect of co-flow on the noise is very significant: at co-flow ratio about 0.2 the noise drops by 5-7 dB fairly uniformly both in the simulations and in the experiment. With $U_{CF} = 0.3U_j$, according to the simulation, the drop reaches 7-9 dB; the new trend for the upstream sound radiation at a ratio of 0.6 will await experimental confirmation.

Finally, the last figure of this section (Fig. 10) illustrates the accuracy of prediction of the noise from the strongly heated jet with co-flow at the experimental conditions of Ref. 6. Although the discrepancy with the experimental data in this case is somewhat larger than for isothermal jets, the effect of co-flow is predicted quite well.

3.4. Simulated nozzle chevrons

An initial step towards technology development using the presumed generality of the non-empirical method consists in adding the effect of nozzle chevrons. The simulation does not incorporate the nozzle; instead, as shown if Fig. 11, the inflow condition is modified (and the grid deformed) to comprise a non-circular shear-layer shape; sources and sinks with zero net mass flow inject a prescribed number of pairs of vortices, N_{chev}. The sources and sinks are positioned at the distance X_{SRC} upstream of the nozzle exit and at the distance R_{SRC} from the nozzle axis. Their polar angles are defined as $\varphi_k = k\Delta\varphi_{chev}$ for the sources and $\tilde{\varphi}_k = (k - 1/2)\Delta\varphi_{chev}$ for the sinks ($k = 1, 2, ..., N_{chev}$; $\Delta\varphi_{chev} = 2\pi/N_{chev}$). Then the changes of the velocity-vector components, Δu_i ($u_1 = u$, $u_2 = v$, $u_3 = w$) induced by the above sources/sinks system at the point $\mathrm{r} = (x, y, z)$ of the nozzle exit plane are given by:

$$\frac{\Delta u_i}{U_j} = \frac{S_{chev}D^2}{4\pi}\sum_{k=1}^{N_{chev}}\left[\frac{x_i - (x_i)^{(k)}_{source}}{\left|\mathrm{r} - \mathrm{r}^{(k)}_{source}\right|^3} - \frac{x_i - (x_i)^{(k)}_{sink}}{\left|\mathrm{r} - \mathrm{r}^{(k)}_{sink}\right|^3}\right],$$

where S_{chev} is the non-dimensional intensity of the sources and sinks.

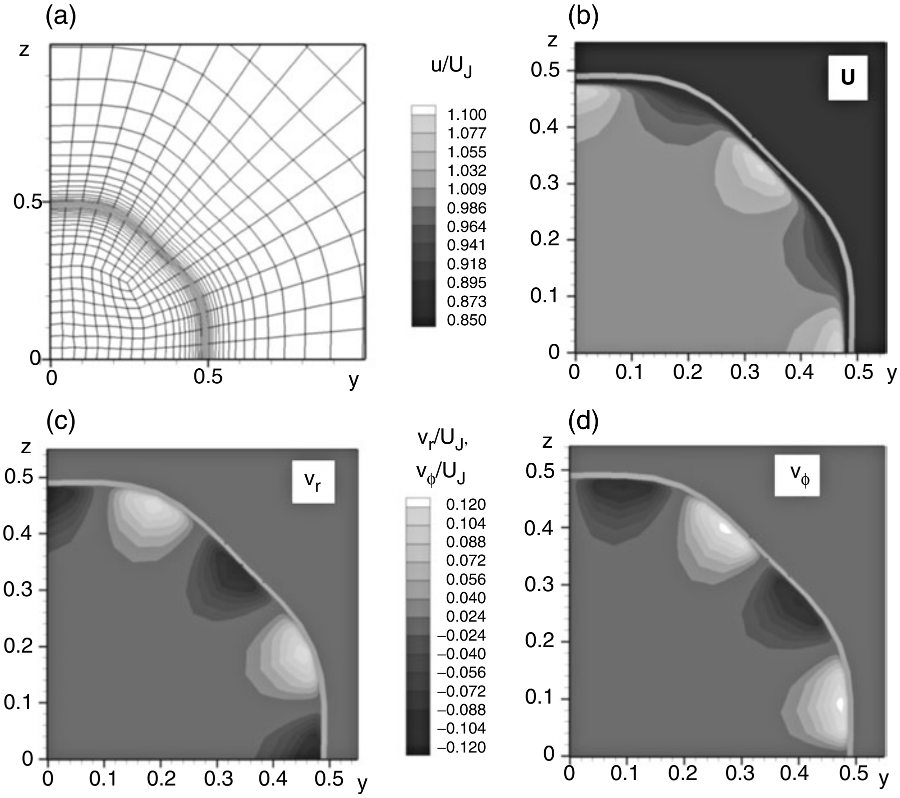

Figure 11. Inflow-plane grid and velocity contours for jet with synthetic chevrons.

The modification of the shape of the nozzle at the exit, aimed at a more realistic imitation of the effect of the chevrons, consists in decreasing the local nozzle radius at the polar angles corresponding to source positions, and increasing it at the angles corresponding to sink positions, with 2% amplitude of deformation. An appropriate smooth deformation of the grid in the vicinity of the nozzle exit is performed as well. The specific parameters of the emulation procedure adjusted on the basis of preliminary RANS computations are as follows: $X_{SRC} = -0.07D$, $R_{SRC} = 0.56D$, $S_{chev} = 0.03$. With $N_{chev} = 8$, these provide plausible comparisons with the core jet flowfield from the core nozzle in flight tests of a Boeing 777, which also had eight chevrons, but a quantitative comparison is not in order, if only because the 777 engine also had a fan flow. The simulation with chevrons is otherwise very close to the baseline, in numerical terms. The grid has 8 points per chevron, in the azimuthal direction. It does not follow the shear layer as well as it does without chevrons, unfortunately; this will be remedied in the future by increasing the number of points.

Figure 12 shows how the jet develops corrugations. These interfere with the early shear-layer instability and with the breakdown of the potential core, which has an effect

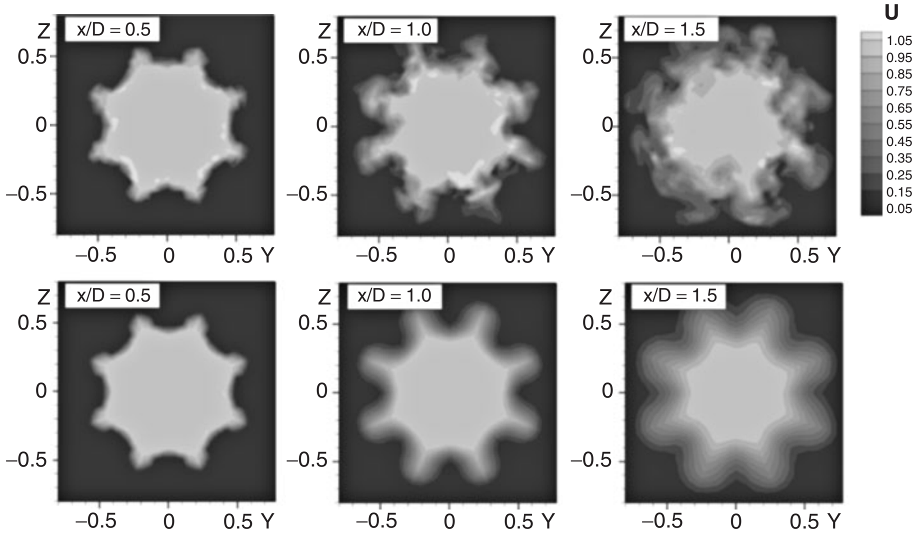

Figure 12. Instantaneous (upper row) and time-average (lower row) axial velocity in cross-flow planes of jet with synthetic chevrons.

on the noise as seen in Fig. 13. The predicted overall level is reduced by up to 2 dB in directions close to the jet axis, which is consistent with experiments. As expected, the drop is caused by a reduction of the low frequency part of the noise (see Fig. 14). At high frequencies ($St > 1.5$), the trend is opposite, which however does not tangibly affect the OASPL. Simulations could assist in designing chevrons that are effective at low frequencies, and not detrimental at medium frequencies. High frequencies will be out of reach for now, which is unfortunate in terms of the true value of these devices in practice. The interaction with other effects, such as heating or shocks, will be explored.

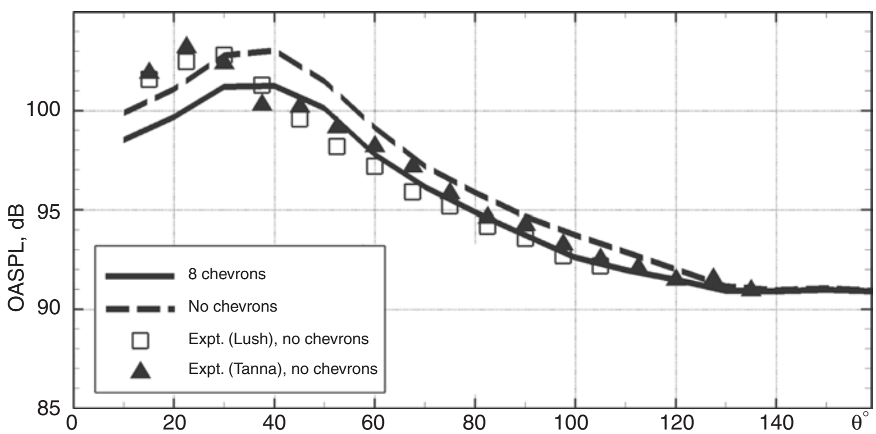

Figure 13. Noise directivity with and without chevrons. Distance 120 diameters.

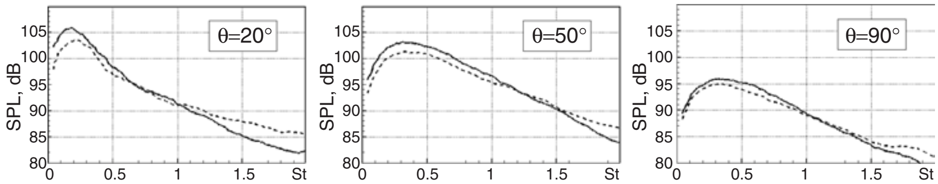

Figure 14. Noise SPL spectra (per unit of Strouhal number) with (dashed lines) and without (solid lines) chevrons. Spectra are averaged over frequency-intervals of $\Delta St = 0.05$. Distance 120 diameters.

3.5. Broadband shock-cells noise of a sonic under-expanded jet

The last effect we are simulating is also of great importance in the airliner industry, and is that of shock cells, which are often present in cruise flight. The shocks, naturally, raise the level of numerical difficulty. The demands of shock capturing and those of LES resolution with acceptable numerical dissipation conflict. Probably for this reason, no examples of LES of jets with shock-cells were found in the literature. However, based on the "numerical schlieren" and density fields from the simulation of Case 16 in *Table 1* shown in Fig. 15, the compromise in the simulations (the local use of flux limiters discussed in Ref. 1) seems to be successful, possibly because the shocks are weak. There are no spurious oscillations, but the shocks are not smeared, and neither is the physical instability suppressed. Shear-layer transition is taking place again, and the motion of the expansion waves and shocks is vivid in animations.

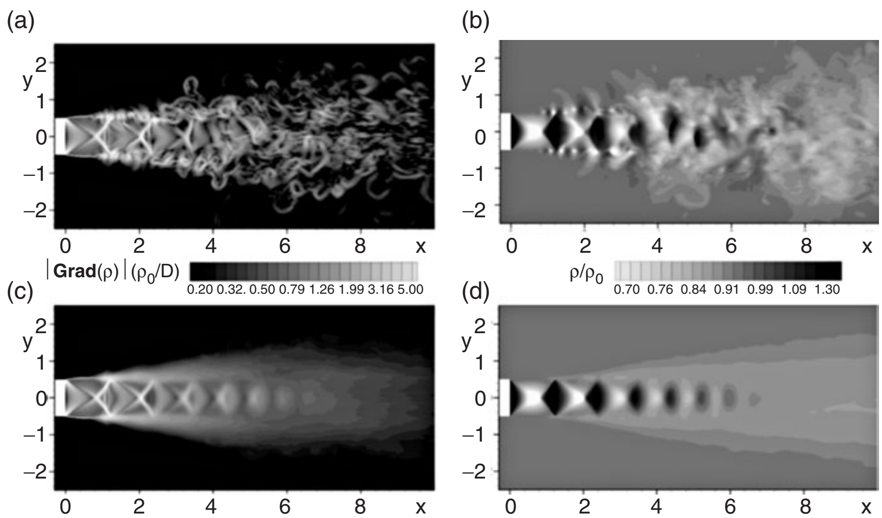

Figure 15. Magnitude of density gradient (a, b), and density (c, d) in sonic under-expanded jet: (a, c) instantaneous; (b, d) time-average.

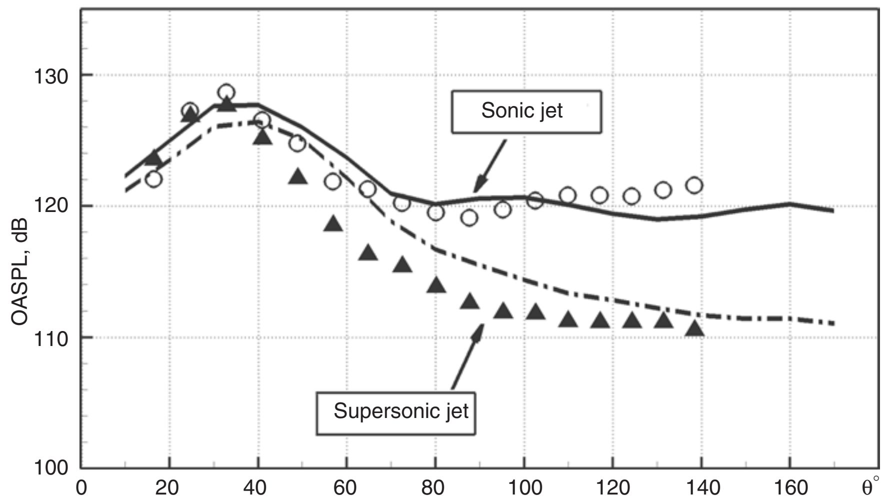

Figure 16. Noise directivity of perfectly expanded supersonic and under-expanded sonic jets. Experiments of Tanna [7]. Distance 72 diameters.

In order to evaluate the impact of the broadband shock-cell component on the total jet noise, similarly to the experiment of Tanna [7], in the present study a direct comparison has been performed of the sonic under-expanded jet with the perfectly-expanded supersonic jet with the same stagnation parameters (Case 15 in *Table 1*). As seen in Fig. 16, the effect of shock cells on the far-field noise is very strong in the lateral direction. The figure also shows that the comparison of the OASPL with experiment does not degrade strongly, relative to subsonic jets, when sonic and supersonic jets are simulated. The disagreement peaks at 4 dB at intermediate of angles, but is often of the order of only 1 or 2 dB. However, as seen in Fig. 17 where both raw (per unit of Strouhal number) and 1/3-octave spectra for the two jets are presented, the good agreement with the data for the sonic jet at relatively small observer angles is reached partially due to error cancellation, namely, an underestimation of the low-frequency part of the spectrum, on one hand, and a sizeable input from spurious peaks at high frequencies, on the other hand. The origin of the peaks is the same as that discussed earlier for subsonic jets, but they are much more pronounced in the sonic jet due to the stabilizing effect of the flow expansion in the initial region (this gives one more incentive for developing a physically sound inflow-forcing concept, as mentioned in Ref. 1). Fortunately, at $\theta > 90°$ where the broadband shock-cell noise is dominant, the frequency range of this noise is not overlapping with the frequencies of the spurious peaks. Consistently with this, the peak frequency of the 1/3-octave spectra at these observer angles compares well with the fit of the experimental data proposed in Ref. 7 (see Fig. 18).

In general, the results seem to be very promising in the context of the airline industry, since noise is a major aspect of competitive advantage, and there is no obstacle to

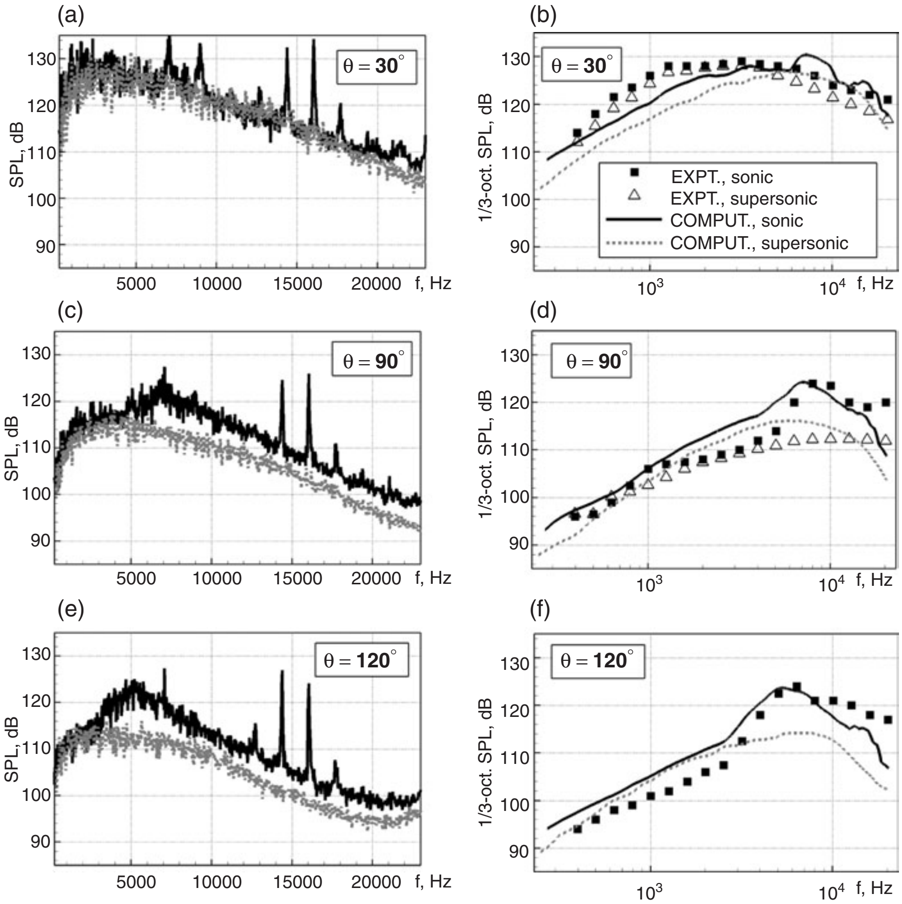

Figure 17. Raw (a – c) and 1/3-octave (d – f) spectra of perfectly expanded supersonic and under-expanded sonic jets at $M_a = 1.372$. Experiments from Ref. 7, for sonic jet, and from Ref. 4 at $M_a = 1.33$, for supersonic jet. Distance 72 diameters.

running a rather complete case with dual streams of appropriate temperatures, each with its shock system.

4. CONCLUSION

The wide range of cases presented here is a good sign in terms of the generality that is the motivation for using LES in spite of its cost. All the essential physical effects such as compressibility and temperature appear to have been explored, several for the first time by LES (for jets and including noise prediction). This was done without presenting a new challenge other than grid count, and required only a backward-compatible upgrade of the sound-calculation system. The simulations responded fairly well to grid

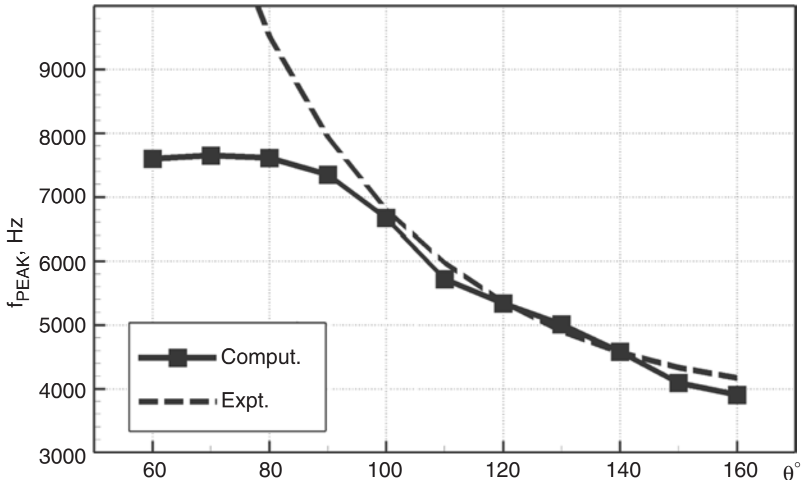

Figure 18. Dependence of peak-frequency of broadband shock-cell noise on observer angle.

refinement by an average factor of 3/4 in each direction, which is modest, but not insignificant when all components of the method are at least second-order accurate. The challenge is now to address still more complete cases, closer to actual engines, and to reduce the "manual" adjustments of the differencing schemes and limiters. A physically-justified inflow forcing device may suppress spurious peaks by making the initial transition more realistic. The strategic choices made both for the LES and for the far-field sound "post-processing" appear vindicated (however, the disablement the SGS model will be reversed at some point, when grids permit it). The frequency range that is accessible to LES remains too narrow, of course, and even runs on super-computers would not come close to covering the audible range. As a result, computational studies will be useful in supporting physical intuition, which is often far from satisfied by experiments which only measure thrust and noise, and in predicting low-frequency noise. The immediate future will lead to dual nozzles, which are standard on airliners, and to deeper studies of shock-cell flows with and without chevrons. Then, simulations with actual nozzle geometries will be initiated.

ACKNOWLEDGEMENTS

This work was primarily funded by Boeing Commercial Airplanes, and partially by General Electric Aircraft Engines, under the supervision of Dr. P. Gliebe.

REFERENCES

[1] Shur, M.L., Strelets, M.Kh., and Spalart, P.R., Noise Prediction for Increasingly Complex Jets. Part I: Methods and Tests, *International Journal of Aeroacoustics*. 2005, 4 (3&4), 213-246.

[2] Shur, M.L., Strelets, M.Kh., and Spalart, P.R., Noise Prediction for Increasingly Complex Jets, *Colloquium EUROMECH 449, Dec 9-12 2003*, Chamonix, France.

[3] Lush, P.A., Measurements of Subsonic Jet Noise and Comparison with Theory, *Journal of Fluid Mechanics*, 1971, 46, 477-500.

[4] Tanna, H.K., An Experimental Study of Jet Noise. Part I: Turbulent Mixing Noise, *Journal of Sound and Vibration*, 1977, 50, 405-428.

[5] Tanna, H.K., and Morris, P.J., In-flight Simulation Experiments on Turbulent Jet Mixing Noise, *Journal of Sound and Vibration*, 1977, 53 (3), 389-405.

[6] Ahuja, K.K., Tanna, H.K., and Tester, B.J., Effect of Simulated Forward Flight on Jet Noise, Shock Noise and Internal Noise, *AIAA Paper*, 1979, AIAA-79-0615.

[7] Tanna, H.K., An Experimental Study of Jet Noise. Part II: Shock Associated Noise, *Journal of Sound and Vibration,* 1977, 50, 429-444.

[8] Hoch, R.G., Duponchel, J.P., Cocking, B.J., and Bryce, W.D., Studies of the Influence of Density on Jet Noise, *Journal of Sound and Vibration*, 1973, 28 (4), 649-668.

[9] Viswanathan, K., Aeroacoustics of Hot Jets, *Journal of Fluid Mechanics*, 2004, 516, 39-82.

[10] Fisher, M.J., Comment on "Jet Mixing Noise from Fine-Scale Turbulence", *AIAA Journal*, 2000, 38 (2), 379.

[11] Tam, C.K.W., and Auriault, L., Reply by the Authors to M.J. Fisher, *AIAA Journal*, 2000, 38 (2), 379-380.

[12] Lau, J.C., Effect of Exit Mach Number and Temperature on Mean-Flow and Turbulence Characteristics in Round Jets, *Journal of Fluid Mechanics*, 1981, 105, 193-218.

[13] Lockwood, F.C., and Moneib, H.A., Fluctuating Temperature Measurements in a Heated Round Jet, *Combustion Science and Technology*, 1980, 22, 63-81.

[14] Simonich, J.C., Narayanan, S., Barber, T.J., and Nishimura, M., High Subsonic Jet Experiments. Part I: Aeroacoustic Characterization, Noise Reduction and Dimensional Scaling Effects, *AIAA Paper*, 2000, AIAA-2000-2022.

[15] Lau, J.C., Morris, P.J., and Fisher, M.J., Measurements in Subsonic and Supersonic Free Jets Using a Laser Velocimeter, *Journal of Fluid Mechanics*, 1979, 93, 1-27.

[16] Zaman, K.B.M., Asymptotic Spreading Rate of Initially Compressible Jets – Experiment and Analysis, *Physics of Fluids*, 1998, 10, 2652-2660.

[17] Morris, P.J., Turbulence Measurements in Subsonic and Supersonic Jets in a Parallel Stream, *AIAA Journal*, 1976, 14 (10), 1468-1475.

[18] Wygnanski, I., and Fiedler, H., Some Measurements in the Self-preserving Jet, *Journal of Fluid Mechanics*, 1969, 38 (3), 577-612.

[19] Michalke, A., and Michel, U., Prediction of Jet Noise in Flight from Static Tests, *Journal of Sound and Vibration*, 1979, 67 (3), 341-367.